Preventing Protein Adsorption and Macrophage Uptake of Gold Nanoparticles *via* a Hydrophobic Shield

Timothy A. Larson,[†] Pratixa P. Joshi,[†] and Konstantin Sokolov[†,‡,*]

[†]Department of Biomedical Engineering, University of Texas at Austin, Austin, Texas 78712, United States and [‡]Department of Imaging Physics, M.D. Anderson Cancer Center, Houston, Texas 77030, United States

ABSTRACT

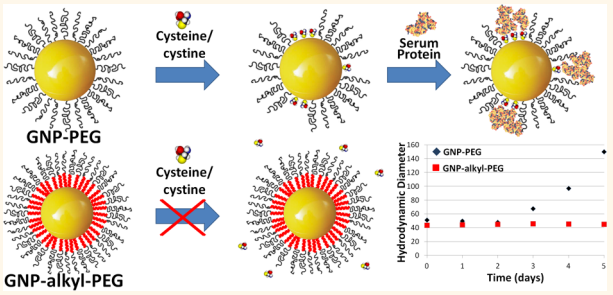

Polyethylene glycol (PEG) surface coatings are widely used to render stealth properties to nanoparticles in biological applications. There is abundant literature on the benefits of PEG coatings and their ability to reduce protein adsorption, to diminish nonspecific interactions with cells, and to improve pharmacokinetics, but very little discussion of the limitations of PEG coatings. Here, we show that physiological concentrations of cysteine and cystine can displace methoxy-PEG-thiol molecules from the gold nanoparticle (GNP) surface that leads to protein adsorption and cell uptake in macrophages within 24 h. Furthermore, we address this problem by incorporating an alkyl linker between the PEG and the thiol moieties that provides a hydrophobic shield layer between the gold surface and the hydrophilic outer PEG layer. The mPEG-alkyl-thiol coating greatly reduces protein adsorption on GNPs and their macrophage uptake. This has important implications for the design of GNP for biological systems.

KEYWORDS: gold nanoparticles · polyethylene glycol · protein adsorption · cellular interaction

Gold nanoparticles (GNPs) have been proposed as optical contrast agents and drug carriers for a variety of biochemical and biomedical applications.[1−12] Their strong and tunable optical properties, in combination with an easily modified surface chemistry, have spurred this interest.[13−17] These applications generally require modifying the surface chemistry in order to render the nanoparticles biocompatible, to provide functionality, and to stabilize the nanoparticle suspension against unwanted aggregation in biological media.[18] A variety of modifications have been investigated for this purpose, including combinations of proteins, self-assembled monolayers of small molecules, and natural or synthetic polymers.[19−24] The polymer polyethylene glycol (PEG), modified to have a thiol group on one end (methoxy-PEG-thiol or mPEG-SH), has found wide use in surface modification due to its lack of toxicity, resistance to protein adsorption, and ease with which it forms monolayers on gold surfaces.[25,26] PEG has been used in drug formulations for decades, and has been shown to increase the blood half-life of a variety of pharmaceutically active compounds without adverse toxic effects.[27]

There have been a number of studies investigating the stability, toxicity, protein, and cellular interactions, and *in vivo* biodistribution of PEGylated gold nanoparticles. Multiple studies have shown that PEGylation reduces protein adsorption and can reduce the cellular uptake of nanoparticles.[28,29] PEGylated gold spheres have been used as negative controls for cellular interaction, demonstrating that PEGylated spheres generally do not bind to a variety of cancer cell lines in the absence of a specific targeting ligand.[6,30,31] An increasing density of PEG molecules on GNPs correlates inversely with adsorption of serum proteins, and the degree of adsorption correlates directly with particle internalization by J774A.1 macrophage cells.[29] However, these *in vitro* experiments often use simplified media that may miss out on more complicated mechanisms of interaction that can occur in blood.[32] Additionally, the studies are usually done with time points of several hours, which can miss slower processes that are relevant to *in vivo* applications.[33]

* Address correspondence to kostia@mail.utexas.edu.

Received for review August 3, 2012 and accepted September 18, 2012.

Published online September 25, 2012
10.1021/nn3035155

In vivo experiments are performed with longer time points ranging from hours to days, with the end point analysis generally consisting of mass spectrometry or another quantitation method to determine the amount of gold in various tissues. It has been widely reported that the liver and spleen accumulate the majority of systemically injected nanoparticles, and that nanoparticle clearance is dependent on both size and surface chemistry.[34−36] PEGylated gold nanoshells were demonstrated as the first plasmonic nanoparticle-based agents for photothermal therapy of a cancer *in vivo*, with their tumor accumulation attributed to the enhanced permeability and retention (EPR) effect.[37] The blood half-life of gold nanorods was improved through PEGylation, and higher densities of PEG molecules resulted in an increase in half-life up to 24 h.[38−40] The addition of mPEG-SH to spherical GNPs conjugated to the tumor necrosis factor (TNF) greatly increased the blood half-life and tumor accumulation of TNF.[41] Several studies have shown that increasing the molecular weight of attached PEG molecules up to 10 kDa leads to a higher blood half-life for spherical gold particles and that increased blood half-life leads to higher tumor accumulation in a mouse xenograft tumor model.[33,42] However, the majority of injected particles is eventually cleared from the blood by the reticuloendothelial system (RES) and the nanoparticles are accumulated in the liver and spleen, even when particles are conjugated only with PEG molecules.

It has been shown that gold nanoparticle conjugates can be destabilized by thiol-containing small molecules. For example, glutathione is a thiol-containing molecule derived from cysteine that is present in concentrations ranging from 1 to 10 mM in the cytosol and at low micromolar concentrations in the blood.[43] Oishi *et al*. relied on intracellular glutathione as an activation agent for a siRNA delivery vehicle comprising a PEGylated gold nanosphere with siRNA bound to the gold surface *via* a thiol bond.[43] Glutathione-mediated displacement of siRNA molecules inside cells led to a high gene knockdown activity of the GNP-siRNA-PEG complex. Several other papers have reported the use of dithiothreitol (DTT) at millimolar concentrations to displace DNA attached to the surface of GNPs in order to facilitate quantitative assays of DNA loading on the nanoparticles.[44,45]

As can be seen from the literature, a PEG layer on nanoparticles can reduce adsorption of serum proteins and can diminish nonspecific cellular interactions; it also increases the blood half-life which can improve the tumor targeting efficiency of a nanoparticle formulation. However, surface coatings formed using thiol conjugation chemistry can be displaced by thiol-containing small molecules, and the essential amino acid cysteine is present in the blood in sufficient concentration to warrant further investigation into the stability of PEGylated gold nanoparticles. Blood concentrations of reduced cysteine have been reported at 10−20 uM levels, while concentrations of the oxidized dimer cystine are much higher at 50−100 uM. An additional 50−100 uM cysteine exists within blood proteins for a total blood cysteine concentration as high as 200−300 uM.[46−51] Some studies do not distinguish between reduced and oxidized forms of cysteine in the blood, which can lead to confusion when cysteine levels are reported. DMEM media contains only cystine at a concentration of 200 uM, although macrophages are known to excrete cysteine in order to regulate immune function.[47]

Here, we show that the mPEG-thiol layer on GNPs can be displaced by cysteine molecules. Furthermore, mPEG-thiol modified GNPs (GNP-PEG) adsorb proteins within 24 h of being placed in cell culture media supplemented with fetal bovine serum (FBS). We demonstrate that protein adsorption can be greatly reduced by including a small alkyl chain as a hydrophobic shield between the GNP surface and the outer hydropholic PEG layer. Finally, protein adsorption on GNP-PEG conjugates correlates with increased uptake by a macrophage cell line, whereas there is no detectable uptake by macrophages of GNPs coated by the mPEG molecules with the hydrophobic shield. This study has important ramifications for the design of gold nanoparticle formulations for use as diagnostic and therapeutic agents both *in vitro* and *in vivo*.

RESULTS AND DISCUSSION

Effect of Cysteine on mPEG-SH Gold Nanoparticle Coating. Citrate-capped gold spheres were synthesized following the Turkevich method by adding sodium citrate to a refluxed solution of chlorauric acid.[52] Recent literature results demonstrate that citrate plays a role both as a precursor to the nucleating reagent and as a buffer to control the pH.[53,54] The reactivity of gold ions increases with decreasing pH, and this effect is responsible for the ellipticity observed with the synthesis of larger particles using the Frens method.[55] Our reaction ratios were controlled such that the synthesis proceeded slowly, requiring approximately 10 min to complete. The resulting gold colloid was characterized by transmission electron microscopy (TEM), optical spectroscopy, and dynamic light scattering (DLS) (Supporting Information Figure S1). The DLS and TEM measurements were in good agreement, with a typical gold core size of 18 nm. The DLS measurements were consistently found to be 1−2 nm larger than the sizes derived from TEM images, which is consistent with a citrate layer causing an increase in the hydrodynamic radius. We assume that the gold nanoparticle synthesis goes to completion with the reaction resulting in a gold particle concentration of 1.64 nM given the size of *ca.* 17 nm as determined by TEM (Supporting Information Figure S1).

To test the impact of cysteine on PEGylated GNPs, the particles were coated with a mixture of 5 kDa

mPEG-SH and FITC-PEG-SH at a 4:1 ratio. The mixture was required to avoid aggregation, as a coating of 100% FITC-PEG-SH resulted in aggregation of GNPs upon centrifugation. This is not unexpected because even though the FITC molecule does not have a strong binding energy with itself, the effect of small binding energies across multiple moieties has been shown to induce aggregation of nanoparticles in other situations.[45] The PEGylated GNPs were resuspended in PBS, and varying amounts of cysteine and a DTT control were added to aliquots of the GNP-PEG-FITC solution, then the fluorescence intensity was recorded over time. DTT was used as a control because of its ability to efficiently displace thiolated compounds from gold surfaces.[44,45] Incubation of GNP-PEG-FITC with DTT at a high concentration resulted in an increase in fluorescence intensity of the suspension that indicates release of the FITC-PEG-SH molecules from gold nanoparticles. The observed increase in fluorescence signal is due to fluorescence quenching near gold surfaces that is well documented.[56,57] The experiment demonstrated that increasing concentrations of cysteine led to increasing amounts of displaced PEG molecules, with a pronounced effect even at a concentration of cysteine as low as 25 uM (Figure 1). On the basis of previously published literature, we assumed that the PEG was completely displaced after 1 h exposure to 47 mM DTT.[44,45,58,59] The fluorescence data in Figure 1 are linearly rescaled to show the percentage of displaced FITC-PEG-SH molecules from 0% displacement for the GNP control sample to 100% displacement for GNPs treated with DTT.

The fact that cysteine readily displaces densely packed mPEG-SH layers on GNP is somewhat surprising given the resistance of PEG coatings to adsorption of large molecules.[29] We determined the density of mPEG-SH molecules on the gold particle surface, using a previously published procedure.[29] Our protocol led to a density of 2.6 PEG/nm^2, which corresponds to the high PEG density particle group (density more than 1 PEG/nm^2) tested by Walkey *et al.*;[29] this density is also consistent with the highest PEG density of 3.5 PEG/nm^2 for 15 nm diameter gold spheres that was reported in the previous study.[29] Some insight into this process can be gained from a review of the literature on ligand exchange mechanisms of the gold–sulfur bond.[60−62] As noted by Caragheorgheopol and Chechik, gold ligand exchange mechanisms showed a "very rich and diverse chemistry".[62] Thiols, thiolates, and disulfides can be involved in ligand exchange reactions with the specific mechanism depending on the ligand pair involved. The final equilibrium point of ligand exchange reactions depends on both the concentration and the nature of the ligands involved, and it can take a long time before equilibrium is achieved.

Conjugates of GNPs with PEG-alkyl-thiols. A recent publication by Maus *et al.* showed that cysteine-terminal peptides can bind directly to the surface of gold nanoparticles precoated with 3 kDa mPEG-SH.[63] This result shows that cysteine-containing peptides are capable of penetrating through a PEG layer and interacting directly with the gold surface of PEG-coated GNPs. This observation is similar to our results with cysteine, which are described above. Maus *et al.* also demonstrated that the penetration effect could be avoided when an alkyl group is inserted between the PEG and the thiol moieties.[63] Here, we assess the impact of a hydrophobic alkyl chain, which we call a hydrophobic shield, between the thiol group and the PEG portion of the polymer molecule on the stabilization of gold nanoparticles in the biological environment that contains small thiolated compounds such as cysteine and cystine. Methoxy-PEG-alkyl-thiol (mPEG-alkyl-SH) was synthesized by reacting a 20-fold molar excess of mercaptododecanoic acid NHS ester (MDDA-NHS) with methoxy-PEG-amine (see Methods for details). Gold nanoparticles were PEGylated by adding either mPEG-SH or mPEG-alkyl-SH molecules to a water suspension of GNPs at room temperature for 30 min followed by purification *via* centrifugation. DLS measurements of the resulting GNP-PEG and GNP-alkyl-PEG in media supplemented with 5% FBS (complete media) are shown in Figure 2. The addition of mPEG-SH and mPEG-alkyl-SH coatings caused a slight red-shift in the plasmon peak position of *ca.* 2 nm and 4 nm and an increase of *ca.* 1.5% and 7.6% in the peak extinction coefficient of coated nanoparticles, respectively

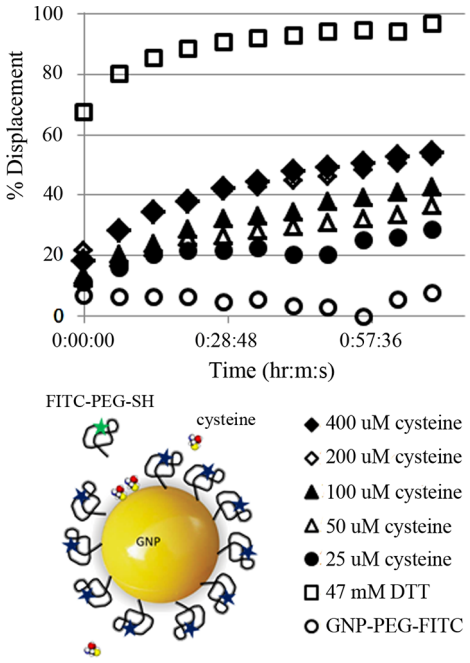

Figure 1. Displacement of FITC-PEG-SH from the GNP surface by solutions with different concentrations of cysteine in PBS as a function of time. Schematic illustrates cysteine displacing FITC-PEG-SH, which leads to increased fluorescence, as indicated by the DTT control. Note that 200 and 400 uM cysteine lines overlap.

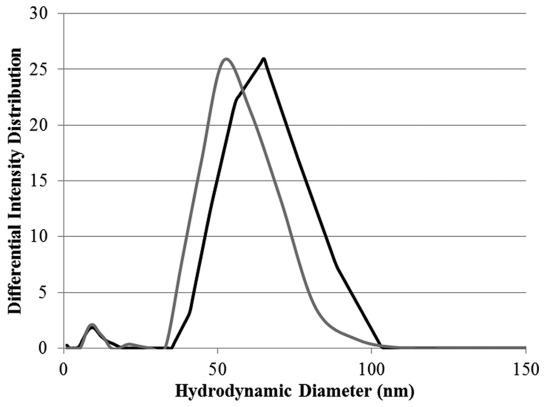

Figure 2. DLS size distribution of freshly prepared GNP-PEG (black, solid line) and GNP-alkyl-PEG (gray, solid line) in complete media.

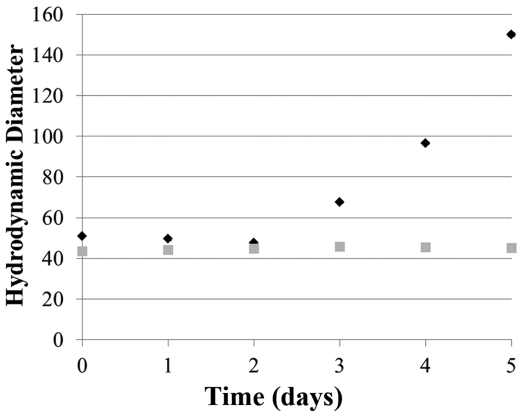

Figure 3. Hydrodynamic diameter of GNP-PEG (black) and GNP-alkyl-PEG (gray) as a function of time over a 5 day period in complete media (DMEM) with 5% FBS. The observed standard deviation was less than 1% of the measured diameters.

(Supporting Information Figure S1). Larger optical changes associated with the mPEG-alkyl-SH layer are attributed to a higher refractive index change on the nanoparticle surface due to the alkyl moiety.

Protein Adsorption on GNP-PEG and GNP-alkyl-PEG. To explore the stability of different PEG coatings in biological media, GNP-PEG and GNP-alkyl-PEG with 10 kDa mPEG moiety were synthesized, washed *via* centrifugation, resuspended in complete media with 5% fetal bovine serum (FBS), and sterile filtered into a clean, sterile cuvette. For these experiments 10 kDa PEG was chosen to match the particle formulation with the longest blood half-life from the data presented by Perrault *et al.*[33] The size of the particles was measured by DLS over a period of 5 days (Figure 3). Cell culture media contains phosphate buffered saline (PBS), a number of divalent cations in the mM range, sulfur containing cystine and methionine, and a few other small molecules that do not have sulfur. FBS adds a much more complicated composition that includes various types of proteins and all of the small molecules found in the nonclotting portion of blood plasma.[64]

The GNP-PEG and GNP-alkyl-PEG showed very different behavior in complete media over the period of 5 days (Figure 3). There was no observable aggregation of either particle type (Supporting Information Figure S2). However, the size of the GNP-PEG began to gradually increase after two days (Figure 3). These changes are likely due to the formation of a protein corona around the particles, a process that was found to proceed gradually over a period of hours and days.[65,66] By contrast, the GNP-alkyl-PEG maintained a constant size during the observation time, indicating that there is far less interactions between the GNP-alkyl-PEG and serum proteins. This result is consistent with our hypothesis that the alkyl group would provide a protective effect in biological media. The effectiveness of the alkyl group is not unexpected, as Maus *et al.* showed that the alkyl group can eliminate the binding of cysteine-terminal peptides to the gold surface.[63] Additionally, mPEG-alkyl-SH was shown to greatly enhance the stability of silver nanoparticles in the presence of high ionic strength solvents.[67]

To further investigate interactions between PEG-coated GNPs and serum proteins we carried out an assay to directly detect protein adsorption on the nanoparticle surface using a Coomassie blue reagent for a Bradford protein assay.[68] GNP-PEG and GNP-alkyl-PEG were suspended in complete media with 5% FBS and were kept in an incubator at 37 °C and 5% CO_2 for 1 day, 3 days, and 5 days. The particles were then washed three times in PBS *via* centrifugation and added to either PBS or the Coomassie Plus reagent from Pierce. The PBS control was used to calculate the concentration of nanoparticles and to obtain gold nanoparticle baseline spectra. The control was also used to monitor the potential aggregation of nanoparticles. Calibration curves showed that the Coomassie Plus assay is sensitive to serum albumin concentrations down to 0.5 ug/mL, which is equivalent to a detection limit of approximately 15 albumin proteins per particle in our experiments (see Supporting Information Figure S3 for representative calibration curves). It is important to note that the protein corona formed on particles in serum contains many different proteins, which can lead to some variability in the response of Coomassie Plus.[29,65,66,69] Control measurements carried out using GNP-PEG and GNP-alkyl-PEG that were not exposed to serum proteins confirmed that the particles alone had a significantly lower effect on the Coomassie Plus reagent when compared to particles incubated in complete media. The supernatant of the final wash step after incubation of nanoparticles with serum also did not show any presence of proteins. Each sample was split into three separate aliquots prior to the initial wash for the Bradford assay. Triplicate measurements on the same particles showed that the Bradford assay had a standard deviation less than 1%, indicating that the majority of the variation in this assay stems from

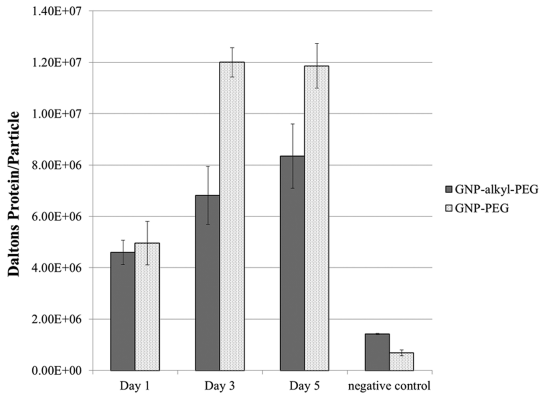

Figure 4. Protein adsorption to GNP-PEG (dotted white) and GNP-alkyl-PEG (gray) over a period of 5 days in complete media with 5% FBS. The negative controls contained particles that had not been exposed to serum.

particle losses during centrifugation. As can be seen in Figure 4, both GNP-PEG and GNP-alkyl-PEG have a significant amount of adsorbed proteins at 24 h, and there is no statistically significant difference in protein adsorption between GNP-PEG and GNP-alkyl-PEG at this early time point. At later time points GNP-PEG has significantly more adsorbed protein than GNP-alkyl-PEG, which agrees with the DLS data shown in Figure 3. It is also interesting to compare the protein adsorption data with the hydrodynamic size radius measurements taken at 24 h. While there is a significant degree of protein adsorption at these time points, it is not immediately obvious in the DLS data. However, a slight increase in the hydrodynamic diameter of the GNP-alkyl-PEG particles of about 3 nm was observed during the first few days (Supporting Information Figure S4). This result suggests that significant adsorption of proteins to GNP-PEG particles may not be easily detectable using DLS and that more direct protein detection methods might be required. Alternately, as the GNP-PEG particles increase in hydrodynamic size between three and five days, there is no observable increase in adsorbed proteins using the Coomassie assay. This is possibly due to the fact that this assay only detects proteins adsorbed with a relatively slow K_{off}, as the washing steps require approximately 3 h in PBS with increasingly dilute serum concentrations. Previously, Casals *et al.* noted the presence of both a hard protein corona and a soft transient protein corona that is detectable by DLS measurements but detaches upon washing.[66] Our DLS measurements and the results of Coomassie assay are consistent with the formation of a similar soft protein corona on top of a harder protein corona on GNP-PEG in media with serum proteins.

Effect of Preincubation in Media on Uptake by Macrophages. After we had shown that cysteine disrupts the mPEG-SH layer on GNP-PEG and that GNP-PEG slowly adsorbs proteins in biological media containing cystine, we carried out experiments to test the effect of the observed protein adsorption on interactions with macrophages.

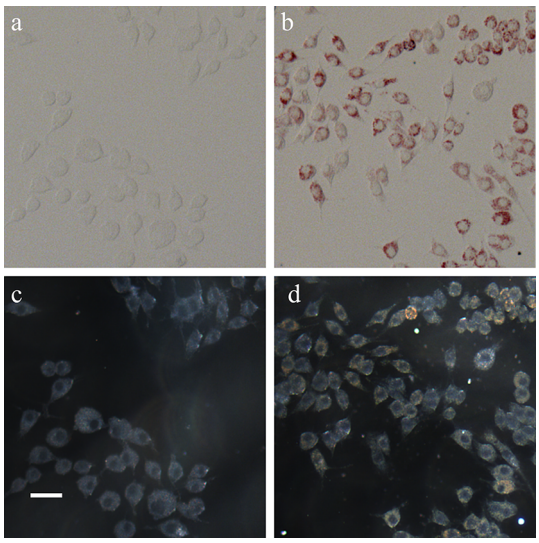

Figure 5. Brightfield (a,b) and darkfield (c,d) images of cells incubated for 4 hours with either freshly prepared GNP-PEG (a,c) or GNP-PEG preincubated in media for 2 days (b,d). Nanoparticles appear red in brightfield transmittance mode and green to orange in darkfield reflectance mode. Scale bar is *ca.* 20 um.

First, we conducted an MTS cell viability assay to determine whether PEGylated GNP or the PEG molecules themselves would have an impact on cell viability at the concentrations used in our experiments.[70] Using pairwise *t* tests, we found that there was no significant difference in cell viability between control and cells incubated with either PEG-coated nanoparticles or PEG molecules (Supporting Information Figure S5).

Initially, we looked at how preincubation of GNP-PEG in media with serum influences their uptake by macrophages (Figure 5). There were no detectable particles in the cells incubated with freshly prepared GNP-PEG particles (Figure 5a,c), in agreement with previous literature reporting no nonspecific interactions at short time points for GNPs with high-density PEG layers.[29] However, significant uptake of nanoparticles was observed after GNP-PEG were first preincubated in media for 2 days and then added to macrophage cells for a period of 4 h (Figure 5b,d). Our results summarized above (see Figures 1, 3 and 4) indicate that preincubation of GNP-PEG in media with serum leads to disruption of the PEG layer by small thiol-containing molecules that results in protein adsorption on the nanoparticle surface. The adsorbed proteins are recognized by macrophage receptors leading to rapid cell uptake. Particles appear red or blue in the brightfield transmitted images depending on their aggregation state, and as various shades of green to orange in the darkfield images (Figure 5). The difference in color between the two imaging modes is caused by the fact that absorption dominates nanoparticle contrast in brightfield images while only scattering is visible in darkfield images of optically thin samples.

Next, a comparison study was conducted using GNP-PEG and GNP-alkyl-PEG preincubated in media for 1 day, 3 days, or 5 days, and then added to cells for 24 h. As seen in Figure 6, there is a very strong uptake in macrophages treated with the GNP-PEG sample while no detectable uptake was observed in cells treated with GNP-alkyl-PEG. The differences in cellular uptake correlate well with the assays comparing both hydrodynamic radius and protein adsorption on GNP-PEG and GNP-alkyl-PEG in complete media (see Figures 3 and 4). It should be noted that there were some degree of protein adsorption to the GNP-alkyl-PEG (Figure 4); this result and the distinct difference in cellular uptake of the two nanoparticles (see Figure 6) suggest that the nature of the protein corona could be more important than the amount of adsorbed proteins in mediating cellular interactions. Additionally, we acquired optical spectra of the particle supernatants after they had been incubated with cells for 1 day (Supporting Information Figures S6 and S7). The supernatant showed that the 1 day preincubated GNP-PEGs underwent some aggregation, but the particles became increasingly stable in the complete media over time with very little aggregation by the 5 day time point (Supporting Information Figure S7). The observed trend can be explained by the evolution of the protein corona over time.[66] It is known that RAW macrophages excrete lysozyme,[71] and that lysozyme can induce aggregation of gold nanoparticles.[72] It is possible that as the protein coating develops around the GNP-PEG during preincubation in complete media they become more resistant to aggregation induced by macrophage secretions. The GNP-alkyl-PEG spectra were very stable and showed no aggregation at any time point, as were the particle solutions prior to addition to cells (Supporting Information Figure S2). The optical microscopy data agree well with the UV−vis spectroscopy of nanoparticle suspensions.

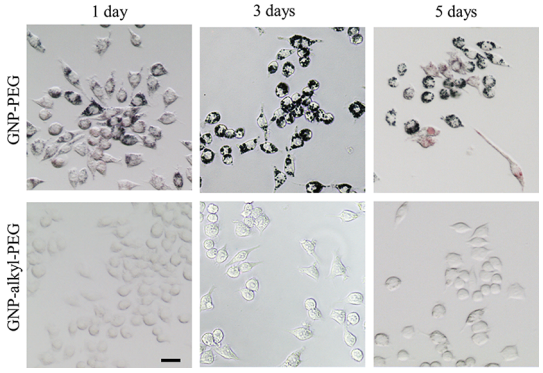

Figure 6. Transmitted brightfield images of cells incubated for 24 h with either GNP-PEG (top row) or GNP-alkyl-PEG (bottom row)). The nanoparticles were preincubated in complete media for 1 day, 3 days, and 5 days. The presence of nanoparticles is readily apparent in cells treated with GNP-PEG as a dark contrast due to light absorption by the particles, while there is no detectable particles visible in the GNP-alkyl-PEG samples. Scale bar is *ca.* 20 um.

CONCLUSIONS

In this study, we analyzed the stability of PEGylated gold nanoparticles in biological media with physiological concentration levels of proteins and small thiolated molecules such as cysteine and cystine. Our data suggest the following mechanism of GNP-PEG destabilization by which GNP-PEGs first have their mPEG-SH coating being slowly displaced over time by cysteine and cystine molecules followed by formation of a

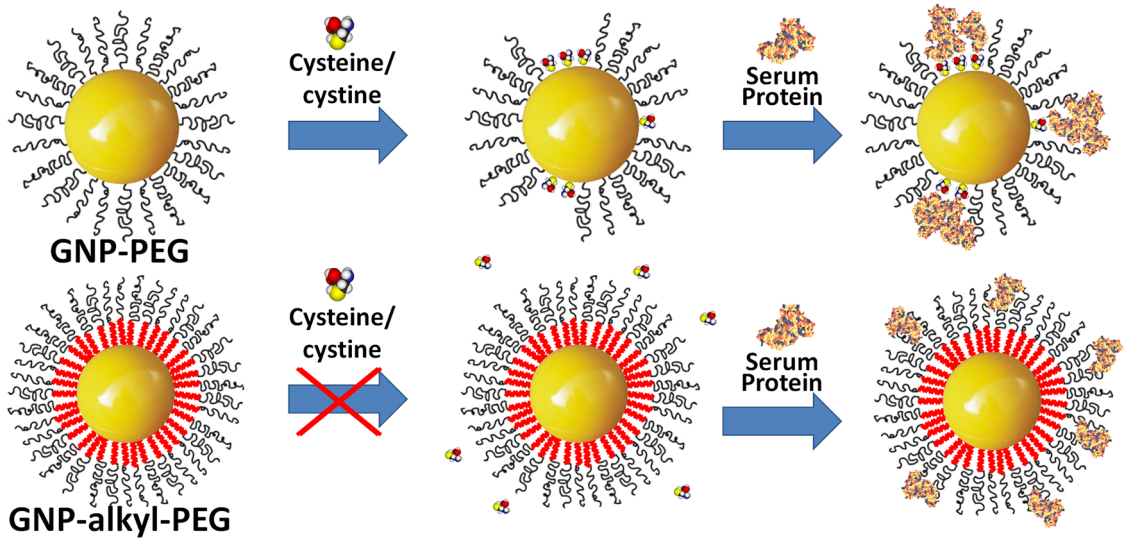

Figure 7. A schematic illustration of the displacement of mPEG-SH molecules in GNP-PEG by small thiolated molecules, for example, cysteine and cysteine, leading to significant adsorption of proteins (upper row). The interactions between nanoparticles and serum proteins is altered when a hydrophobic shield is inserted between the thiol moiety and the outer mPEG layer in GNP-alkyl-PEG (bottom row). The hydrophobic shield drastically reduces nonspecific interactions of the GNP-alkyl-PEG with macrophages.

protein corona that mediates strong interactions with macrophages (Figure 7, top row). We showed that cell uptake can be greatly reduced by incorporating a small hydrophobic shield in between the nanoparticle core and the hydrophilic PEG shell (Figure 7, bottom row). The impact of this PEG modification on the blood half-life of gold nanoparticles is currently being investigated.

MATERIALS AND METHODS

Materials. All reagents were purchased from Sigma-Aldrich unless mentioned otherwise, and used without further purification. Purified 18.2 MΩ water was obtained using a Millipore Direct-Q 3 system. Methoxy-PEG-thiol, 5 kDa and 10 kDa, was obtained from Creative PEGworks. Coomassie Plus Protein Assay Reagent for use in the Bradford assay was purchased from Pierce.

Instrumentation. Dynamic light scattering measurements were carried out using disposable cuvettes in a DelsaNano (Beckman Coulter). Size distribution reconstructions were obtained using the supplied NNLS algorithm. The cumulants analysis in the DelsaNano software package was used to obtain the average sizes in the week long study. Each size measurement was done using 300 acquisitions and 3 repetitions to ensure that the DLS measurements were reproducible. UV−vis measurements and fluorescence kinetic data were acquired using an HT Synergy Plate Reader. Microscopy images were collected on a Leica 6000DM upright microscope using a 20× objective and a SPOT color imaging camera. A halogen and a Xe lamps were used to collect bright-field transmittance and dark-field reflectance images, respectively, from samples on coverslips. A total of 24 well plates were imaged directly on an inverted Leica DM3000 B microscope with a Leica DFC290 camera, a 20× objective, and a halogen lamp.

Synthesis of mPEG-alkyl-SH and PEGylation of GNPs. We used a reaction protocol that was based on standard NHS cross-linking reactions available from Pierce. Methoxy-PEG-thiol (mPEG-SH) was dissolved in water at 500 uM and stored at −20 °C. A mPEG-alkyl-SH was synthesized using a mercaptododecanoic acid *n*-hydroxysuccinimidyl ester (MDDA-NHS, Sigma) and a 10 kDa methoxy-PEG-amine. The MDDA-NHS was dissolved in dimethyl formamide at 100 mM concentration. Then, 200 uL of MDDA-NHS was added to 2 mL of an aqueous solution of methoxy-PEG-amine at 1 mM. A significant amount of precipitate formed upon the addition of MDDA-NHS to the aqueous solution, which is commonly observed when hydrophobic NHS molecules are added to aqueous solutions. The reaction was left overnight, and then the 2 mL solution was dialyzed twice against 1.5 L of water to remove excess MDDA-NHS. The remaining precipitated MUDA-NHS was removed *via* centrifugation at 18000*g* for 30 min, and the supernatant containing methoxy-PEG-alkyl-thiol was aliquoted and stored at −20 °C.

Modification of GNPs with either mPEG-SH or mPEG-alkyl-SH was accomplished by adding either one of the PEG stock solutions to the GNP solution (1.64 nM) to reach the final PEG concentration of 24 uM. The reaction mixture was incubated at room temperature for 30 min, and then GNP-PEGs or GNP-alkyl-PEGs were centrifuged at 14000*g* for 60 min at 4 °C. The pellets containing nanoparticles were redispersed in either cell culture media (DMEM supplemented with 5% FBS) or phosphate buffered saline (PBS) for future studies.

The density of mPEG-SH on GNPs was assayed using the reduction of 5,5′-dithiobis(2-nitrobenzoic acid) (Ellman's reagent, Pierce). Briefly, gold nanoparticles were pelleted by centrifugation after incubation with mPEG-SH, and the concentration of free mPEG-SH molecules in the supernatant was compared to a control solution of mPEG-SH that was not incubated with nanoparticles. The total amount of PEG molecules adsorbed on nanoparticles was obtained by subtracting the amount of mPEG-SH in the supernatant solution from the control mPEG-SH solution. Then the PEG density was calculated by dividing the total amount of adsorbed PEG molecules by the number of nanoparticles and an average surface area of a single nanoparticle.

Fluorescence Kinetics Assay. GNP-PEG-FITC was synthesized by mixing GNP with a mixture of mPEG-SH (5 kDa, Creative PEGworks) and FITC-PEG-SH (5 kDa, Nanocs) at a ratio of 4:1 mPEG:FITC-PEG, and left to react for 30 min. The mixture was used to prevent aggregation during the centrifugation washing step (12000*g*, 60 min), after which nanoparticles were resuspended in PBS. Small aliquots of either cysteine, DTT, or PBS were placed in wells of a black fluorescence 96 well plate, and then the same amount of GNP-PEG-FITC solution in PBS was rapidly added to each well and a fluorescence kinetics assay was begun on the HT Synergy plate reader. The 475−495 nm excitation and the 518−538 nm emission filters were used for measurements of FITC fluorescence.

Protein Adsorption Assays. All GNP samples were sterile-filtered through a 0.2 μm filter. Particles for DLS measurements were placed in a sterilized plastic cuvette with the top covered in foil, wrapped in parafilm to prevent contamination, and then measured daily. There was no observed precipitation or aggregation of nanoparticles as can be seen in Supporting Information, Figure S2.

Particles used in the Bradford assay were split into three separate 400 uL aliquots prior to incubation in complete media. At each time point (1, 3, or 5 days) the particles were washed in PBS three times, with dilution of the pellet out to 5 mL during each step. This washing was required to sufficiently remove all media proteins. After the final washing step the particles were resuspended in 200 uL of PBS, and then three separate 150 uL aliquots were mixed with 150 uL of Coomassie Plus reagent as received from Pierce. Particle only controls were prepared by mixing 50 uL of each GNP sample with 250 uL of PBS to account for potential losses during centrifugation. The spectra of the particle controls were subtracted from the spectra of the particles mixed with Coomassie reagent. Calibration curves were generated using a series dilution of the serum albumin provided with the Coomassie Plus kit from Pierce

Cell Culture and Media experiments. Cells were grown and passaged in DMEM media supplemented with 5% FBS. All experiments with nanoparticles were conducted in phenol-free media. The initial assays with GNP-PEG were carried out using coverslips. Coverslips were sterilized in 70% ethanol, rinsed in a sterile PBS, and then placed in 6 well plates. Each well was seeded at 200,000 cells/well and left to grow overnight. The old media was removed and then 1 mL of either fresh or preincubated GNP-PEGs at 1.4 nM were added to the cells for 4 h.

Twenty four hours assays with GNP-PEGs and GNP-alkyl-PEGs were conducted in triplicate in 24 well plates with 3 samples per particle per time point. For this assay, cells were seeded at 50,000 cells/well. 400 uL of each particle sample at 1.64 nM was incubated with cells for 24 h prior to optical imaging.

The viability assay was conducted on a 96 well plate. Each sample was run in six replicates. Cells were seeded at 5000 cells/well, left to grow overnight, and then incubated with either media, GNP-PEG, GNP-alkyl-PEG, or the mPEG-SH and mPEG-alkyl-SH molecules. The nanoparticles were used at stock concentration of *ca.* 1.64 nM and PEG molecules at concentrations of 10 nM and 1 uM; the upper concentration of PEG molecules was chosen to approximately match concentration of PEG molecules conjugated to 1.64 nM solution of 17 nm diameter particles according to a published data on PEG density on GNP.[29] Cells were washed in media, 100 uL of fresh media was added to each well, then a background absorbance was acquired at 490 nm. MTS reagent (3-(4,5-dimethylthiazol-2-yl)-5-(3-carboxymethoxyphenyl)-2-(4-sulfophenyl)-2H-tetrazolium) was prepared at 2 mg/mL in PBS and phenazine methosulfate (PMS) was prepared at 0.92 mg/mL in PBS. The MTS and PMS solutions were mixed in a 20:1 ratio, then 20 uL of

this mixture was added to each well and allowed to react for 3 h before measurements were taken at 490 nm. The background absorbance was subtracted and the optical density of each sample was normalized relative to the cell only control.

Conflict of Interest: The authors declare no competing financial interest.

Acknowledgment. This work was supported in part by the National Institute of Health Grants RO1 EB008101 and R21 CA135315. The authors thank M. Bolhouse for figure composition and K. Homan proof reading the manuscript.

Supporting Information Available: Supporting Figures S1 to S7 as described in the text. This material is available free of charge *via* the Internet at http://pubs.acs.org.

REFERENCES AND NOTES

1. Ghosh, P.; Han, G.; De, M.; Kim, C. K.; Rotello, V. M. Gold Nanoparticles in Delivery Applications. *Adv. Drug Delivery Rev.* **2008**, *60*, 1307–1315.
2. Huang, X.; Jain, P. K.; El-Sayed, I. H.; El-Sayed, M. A. Gold Nanoparticles: Interesting Optical Properties and Recent Applications in Cancer Diagnostics and Therapy. *Nanomedicine* **2007**, *2*, 681–693.
3. Sokolov, K.; Follen, M.; Aaron, J.; Pavlova, I.; Malpica, A.; Lotan, R.; Richards-Kortum, R. Real-Time Vital Optical Imaging of Precancer Using Anti-Epidermal Growth Factor Receptor Antibodies Conjugated to Gold Nanoparticles. *Cancer Res.* **2003**, *63*, 1999–2004.
4. Skala, M. C.; Crow, M. J.; Wax, A.; Izatt, J. A. Photothermal Optical Coherence Tomography of Epidermal Growth Factor Receptor in Live Cells Using Immunotargeted Gold Nanospheres. *Nano Lett.* **2008**, *8*, 3461–3467.
5. Rana, S.; Bajaj, A.; Mout, R.; Rotello, V. M. Monolayer Coated Gold Nanoparticles for Delivery Applications. *Adv. Drug Delivery Rev.* **2012**, *64*, 200–216.
6. Mallidi, S.; Larson, T.; Aaron, J.; Sokolov, K.; Emelianov, S. Molecular Specific Optoacoustic Imaging with Plasmonic Nanoparticles. *Opt. Express* **2007**, *15*, 6583–6588.
7. Li, W.; Cai, X.; Kim, C.; Sun, G.; Zhang, Y.; Deng, R.; Yang, M.; Chen, J.; Achilefu, S.; Wang, L. V.; *et al.* Gold Nanocages Covered with Thermally-Responsive Polymers for Controlled Release by High-Intensity Focused Ultrasound. *Nanoscale* **2011**, *3*, 1724–1730.
8. Dykman, L.; Khlebtsov, N. Gold Nanoparticles in Biomedical Applications: Recent Advances and Perspectives. *Chem. Soc. Rev.* **2012**, *41*, 2256–2282.
9. Dreaden, E. C.; Austin, L. A.; Mackey, M. A.; El-Sayed, M. A. Size Matters: Gold Nanoparticles in Targeted Cancer Drug Delivery. *Ther. Delivery* **2012**, *3*, 457–478.
10. Curry, A.; Crow, M. J.; Wax, A. Molecular Imaging of Epidermal Growth Factor Receptor in Live Cells with Refractive Index Sensitivity Using Dark-Field Microspectroscopy and Immunotargeted Nanoparticles. *J. Biomed. Opt.* **2008**, *13*, 014022/1–014022/7.
11. Chanda, N.; Kattumuri, V.; Shukla, R.; Zambre, A.; Katti, K.; Upendran, A.; Kulkarni, R. R.; Kan, P.; Fent, G. M.; Casteel, S. W.; *et al.* Bombesin Functionalized Gold Nanoparticles Show *in Vitro* and *in Vivo* Cancer Receptor Specificity. *Proc. Natl. Acad. Sci. U.S.A.* **2010**, *107*, 8760–8765.
12. Aaron, J.; Nitin, N.; Travis, K.; Kumar, S.; Collier, T.; Park, S. Y.; Jose-Yacaman, M.; Coghlan, L.; Follen, M.; Richards-Kortum, R.; *et al.* Plasmon Resonance Coupling of Metal Nanoparticles for Molecular Imaging of Carcinogenesis *in Vivo*. *J. Biomed. Opt.* **2007**, *12*, 034007/1–034007/11.
13. Tkachenko, A. G.; Xie, H.; Coleman, D.; Glomm, W.; Ryan, J.; Anderson, M. F.; Franzen, S.; Feldheim, D. L. Multifunctional Gold Nanoparticle–Peptide Complexes for Nuclear Targeting. *J. Am. Chem. Soc.* **2003**, *125*, 4700–4701.
14. Kim, D.; Jeong, Y. Y.; Jon, S. A Drug-Loaded Aptamer–Gold Nanoparticle Bioconjugate for Combined CT Imaging and Therapy of Prostate Cancer. *ACS Nano* **2010**, *4*, 3689–3696.
15. Jain, P. K.; Lee, K. S.; El-Sayed, I. H.; El-Sayed, M. A. Calculated Absorption and Scattering Properties of Gold Nanoparticles of Different Size, Shape, and Composition: Applications in Biological Imaging and Biomedicine. *J. Phys. Chem. B* **2006**, *110*, 7238–7248.
16. Seekell, K.; Crow, M. J.; Marinakos, S.; Ostrander, J.; Chilkoti, A.; Wax, A. Hyperspectral Molecular Imaging of Multiple Receptors Using Immunolabeled Plasmonic Nanoparticles. *J. Biomed. Opt.* **2011**, *16*, 116003/116001–116003/116012.
17. Young, J. K.; Figueroa, E. R.; Drezek, R. A. Tunable Nanostructures as Photothermal Theranostic Agents. *Ann. Biomed. Eng.* **2012**, *40*, 438–459.
18. Albanese, A.; Chan, W. C. W. Effect of Gold Nanoparticle Aggregation on Cell Uptake and Toxicity. *ACS Nano* **2011**, *5*, 5478–5489.
19. Corbierre, M. K.; Cameron, N. S.; Sutton, M.; Mochrie, S. G. J.; Lurio, L. B.; Rühm, A.; Lennox, R. B. Polymer-Stabilized Gold Nanoparticles and Their Incorporation into Polymer Matrices. *J. Am. Chem. Soc.* **2001**, *123*, 10411–10412.
20. Zhao, W.; Brook, M. A.; Li, Y. Design of Gold Nanoparticle-Based Colorimetric Biosensing Assays. *ChemBioChem* **2008**, *9*, 2363–2371.
21. Krpetić, Z. e.; Nativo, P.; Porta, F.; Brust, M. A Multidentate Peptide for Stabilization and Facile Bioconjugation of Gold Nanoparticles. *Bioconjugate Chem.* **2009**, *20*, 619–624.
22. Kumar, S.; Aaron, J.; Sokolov, K. V. Directional Conjugation of Antibodies to Nanoparticles for Synthesis of Multiplexed Optical Contrast Agents with Both Delivery and Targeting Moieties. *Nat. Protoc.* **2008**, *3*, 314–320.
23. Nune, S. K.; Chanda, N.; Shukla, R.; Katti, K.; Kulkarni, R. R.; Thilakavathy, S.; Mekapothula, S.; Kannan, R.; Katti, K. V. Green Nanotechnology from Tea: Phytochemicals in Tea as Building Blocks for Production of Biocompatible Gold Nanoparticles. *J. Mater. Chem.* **2009**, *19*, 2912–2920.
24. Tam, N. C. M.; Scott, B. M. T.; Voicu, D.; Wilson, B. C.; Zheng, G. Facile Synthesis of Raman Active Phospholipid Gold Nanoparticles. *Bioconjugate Chem.* **2010**, *21*, 2178–2182.
25. Shon, Y.-S.; Mazzitelli, C.; Murray, R. W. Unsymmetrical Disulfides and Thiol Mixtures Produce Different Mixed Monolayer-Protected Gold Clusters. *Langmuir* **2001**, *17*, 7735–7741.
26. Eck, W.; Craig, G.; Sigdel, A.; Ritter, G.; Old, L. J.; Tang, L.; Brennan, M. F.; Allen, P. J.; Mason, M. D. Pegylated Gold Nanoparticles Conjugated to Monoclonal F19 Antibodies as Targeted Labeling Agents for Human Pancreatic Carcinoma Tissue. *ACS Nano* **2008**, *2*, 2263–2272.
27. Knop, K.; Hoogenboom, R.; Fischer, D.; Schubert, U. S. Poly(Ethylene Glycol) in Drug Delivery: Pros and Cons as Well as Potential Alternatives. *Angew. Chem., Int. Ed.* **2010**, *49*, 6288–6308.
28. Arnida; Malugin, A.; Ghandehari, H. Cellular Uptake and Toxicity of Gold Nanoparticles in Prostate Cancer Cells: A Comparative Study of Rods and Spheres. *J. Appl. Toxicol.* **2010**, *30*, 212–217.
29. Walkey, C. D.; Olsen, J. B.; Guo, H.; Emili, A.; Chan, W. C. W. Nanoparticle Size and Surface Chemistry Determine Serum Protein Adsorption and Macrophage Uptake. *J. Am. Chem. Soc.* **2011**, *134*, 2139–2147.
30. Larson, T.; Bankson, J. A.; Aaron, J.; Sokolov, K. Hybrid Plasmonic Magnetic Nanoparticles as Molecular Specific Agents for Mri/Optical Imaging and Photothermal Therapy of Cancer Cells. *Nanotechnology* **2007**, *18*, 325101/1–325101/8.
31. Mallidi, S.; Larson, T.; Tam, J.; Joshi, P. P.; Karpiouk, A.; Sokolov, K.; Emelianov, S. Multiwavelength Photoacoustic Imaging and Plasmon Resonance Coupling of Gold Nanoparticles for Selective Detection of Cancer. *Nano Lett.* **2009**, *9*, 2825–2831.
32. Walkey, C. D.; Chan, W. C. W. Understanding and Controlling the Interaction of Nanomaterials with Proteins in a Physiological Environment. *Chem. Soc. Rev.* **2012**, *41*, 2780–2799.
33. Perrault, S. D.; Walkey, C.; Jennings, T.; Fischer, H. C.; Chan, W. C. W. Mediating Tumor Targeting Efficiency of Nanoparticles through Design. *Nano Lett.* **2009**, *9*, 1909–1915.

34. Brannon-Peppas, L.; Blanchette, J. O. Nanoparticle and Targeted Systems for Cancer Therapy. *Adv. Drug Delivery Rev.* **2004**, *56*, 1649–1659.
35. Choi, C. H. J.; Alabi, C. A.; Webster, P.; Davis, M. E. Mechanism of Active Targeting in Solid Tumors with Transferrin-Containing Gold Nanoparticles. *Proc. Natl. Acad. Sci. U.S.A.* **2010**, *107*, 1235–1240.
36. Soo Choi, H.; Liu, W.; Misra, P.; Tanaka, E.; Zimmer, J. P.; Itty Ipe, B.; Bawendi, M. G.; Frangioni, J. V. Renal Clearance of Quantum Dots. *Nat. Biotechnol.* **2007**, *25*, 1165–1170.
37. Hirsch, L. R.; Stafford, R. J.; Bankson, J. A.; Sershen, S. R.; Rivera, B.; Price, R. E.; Hazle, J. D.; Halas, N. J.; West, J. L. Nanoshell-Mediated Near-Infrared Thermal Therapy of Tumors under Magnetic Resonance Guidance. *Proc. Natl. Acad. Sci. U.S.A.* **2003**, *100*, 13549–13554.
38. Niidome, T.; Yamagata, M.; Okamoto, Y.; Akiyama, Y.; Takahashi, H.; Kawano, T.; Katayama, Y.; Niidome, Y. PEG-Modified Gold Nanorods with a Stealth Character for *in Vivo* Applications. *J. Controlled Release* **2006**, *114*, 343–347.
39. Akiyama, Y.; Mori, T.; Katayama, Y.; Niidome, T. The Effects of PEG Grafting Level and Injection Dose on Gold Nanorod Biodistribution in the Tumor-Bearing Mice. *J. Controlled Release* **2009**, *139*, 81–84.
40. von Maltzahn, G.; Park, J.-H.; Agrawal, A.; Bandaru, N. K.; Das, S. K.; Sailor, M. J.; Bhatia, S. N. Computationally Guided Photothermal Tumor Therapy Using Long-Circulating Gold Nanorod Antennas. *Cancer Res.* **2009**, *69*, 3892–3900.
41. Paciotti, G. F.; Myer, L.; Weinreich, D.; Goia, D.; Pavel, N.; McLaughlin, R. E.; Tamarkin, L. Colloidal Gold: A Novel Nanoparticle Vector for Tumor Directed Drug Delivery. *Drug Delivery* **2004**, *11*, 169–183.
42. Lipka, J.; Semmler-Behnke, M.; Sperling, R. A.; Wenk, A.; Takenaka, S.; Schleh, C.; Kissel, T.; Parak, W. J.; Kreyling, W. G. Biodistribution of PEG-Modified Gold Nanoparticles Following Intratracheal Instillation and Intravenous Injection. *Biomaterials* **2010**, *31*, 6574–6581.
43. Oishi, M.; Nakaogami, J.; Ishii, T.; Nagasaki, Y. Smart PEGylated Gold Nanoparticles for the Cytoplasmic Delivery of siRNA to Induce Enhanced Gene Silencing. *Chem. Lett.* **2006**, *35*, 1046–1047.
44. Li, N.; Larson, T.; Nguyen, H. H.; Sokolov, K. V.; Ellington, A. D. Directed Evolution of Gold Nanoparticle Delivery to Cells. *Chem. Commun. (Cambridge, U. K.)* **2010**, *46*, 392–394.
45. Sato, K.; Hosokawa, K.; Maeda, M. Non-Cross-Linking Gold Nanoparticle Aggregation as a Detection Method for Single-Base Substitutions. *Nucleic Acids Res.* **2005**, *33*, e4.
46. Dröge, W.; Eck, H. P.; Gmünder, H.; Mihm, S. Modulation of Lymphocyte Functions and Immune Responses by Cysteine and Cysteine Derivatives. *Am. J. Med.* **1991**, *91*, S140–S144.
47. Gmunder, H.; Eck, H. P.; Benninghoff, B.; Roth, S.; Droge, W. Macrophages Regulate Intracellular Glutathione Levels of Lymphocytes. Evidence for an Immunoregulatory Role of Cysteine. *Cell. Immunol.* **1990**, *129*, 32–46.
48. Jacob, N.; Bruckert, E.; Giral, P.; Foglietti, M. J.; Turpin, G. Cysteine Is a Cardiovascular Risk Factor in Hyperlipidemic Patients. *Atherosclerosis* **1999**, *146*, 53–59.
49. Muller, F.; Svardal, A.; Aukrust, P.; Berge, R.; Ueland, P.; Froland, S. Elevated Plasma Concentration of Reduced Homocysteine in Patients with Human Immunodeficiency Virus Infection. *Am. J. Clin. Nutr.* **1996**, *63*, 242–248.
50. Murphy, G.; Fan, J.-H.; Mark, S. D.; Dawsey, S. M.; Selhub, J.; Wang, J.; Taylor, P. R.; Qiao, Y.-L.; Abnet, C. C. Prospective Study of Serum Cysteine Levels and Oesophageal and Gastric Cancers in China. *Gut* **2011**, *60*, 618–623.
51. Özkan, Y.; Özkan, E.; Şimşek, B. Plasma Total Homocysteine and Cysteine Levels as Cardiovascular Risk Factors in Coronary Heart Disease. *Int. J. Cardiol.* **2002**, *82*, 269–277.
52. Turkevich, J.; Stevenson, P. C.; Hillier, J. The Formation of Colloidal Gold. *J. Phys. Chem.* **1953**, *57*, 670–673.
53. Ji, X.; Song, X.; Li, J.; Bai, Y.; Yang, W.; Peng, X. Size Control of Gold Nanocrystals in Citrate Reduction: The Third Role of Citrate. *J. Am. Chem. Soc.* **2007**, *129*, 13939–13948.
54. Ojea-Jiménez, I.; Bastús, N. G.; Puntes, V. Influence of the Sequence of the Reagents Addition in the Citrate-Mediated Synthesis of Gold Nanoparticles. *J. Phys. Chem. C* **2011**, *115*, 15752–15757.
55. Frens, G. Controlled Nucleation for the Regulation of the Particle Size in Monodisperse Colloid Suspensions. *Nature* **1973**, *241*, 20–22.
56. Zheng, D.; Seferos, D. S.; Giljohann, D. A.; Patel, P. C.; Mirkin, C. A. Aptamer Nano-flares for Molecular Detection in Living Cells. *Nano Lett.* **2009**, *9*, 3258–3261.
57. Schneider, G.; Decher, G.; Nerambourg, N.; Praho, R.; Werts, M. H. V.; Blanchard-Desce, M. Distance-Dependent Fluorescence Quenching on Gold Nanoparticles Ensheathed with Layer-by-Layer Assembled Polyelectrolytes. *Nano Lett.* **2006**, *6*, 530–536.
58. Yi, D. K.; Sun, I.-C.; Ryu, J. H.; Koo, H.; Park, C. W.; Youn, I.-C.; Choi, K.; Kwon, I. C.; Kim, K.; Ahn, C.-H. Matrix Metalloproteinase Sensitive Gold Nanorod for Simultaneous Bioimaging and Photothermal Therapy of Cancer. *Bioconjugate Chem.* **2010**, *21*, 2173–2177.
59. Lee, S.; Cha, E.-J.; Park, K.; Lee, S.-Y.; Hong, J.-K.; Sun, I.-C.; Kim, S. Y.; Choi, K.; Kwon, I. C.; Kim, K.; *et al*. A Near-Infrared-Fluorescence-Quenched Gold-Nanoparticle Imaging Probe for *in Vivo* Drug Screening and Protease Activity Determination. *Angew. Chem.* **2008**, *120*, 2846–2849.
60. Grönbeck, H.; Curioni, A.; Andreoni, W. Thiols and Disulfides on the Au(111) Surface: The Headgroup−Gold Interaction. *J. Am. Chem. Soc.* **2000**, *122*, 3839–3842.
61. Reyes, E. n.; Madueño, R.; Blázquez, M.; Pineda, T. Facile Exchange of Ligands on the 6-Mercaptopurine-Monolayer Protected Gold Clusters Surface. *J. Phys. Chem. C* **2010**, *114*, 15955–15962.
62. Caragheorgheopol, A.; Chechik, V. Mechanistic Aspects of Ligand Exchange in Au Nanoparticles. *Phys. Chem. Chem. Phys.* **2008**, *10*, 5029–5041.
63. Maus, L.; Dick, O.; Bading, H.; Spatz, J. P.; Fiammengo, R. Conjugation of Peptides to the Passivation Shell of Gold Nanoparticles for Targeting of Cell-Surface Receptors. *ACS Nano* **2010**, *4*, 6617–6628.
64. Marazzi, J.; Kleyer, J.; Paredes, J. M. V.; Gertsch, J. Endocannabinoid Content in Fetal Bovine Sera—Unexpected Effects on Mononuclear Cells and Osteoclastogenesis. *J. Immunol. Methods* **2011**, *373*, 219–228.
65. Lundqvist, M.; Stigler, J.; Cedervall, T.; Berggård, T.; Flanagan, M. B.; Lynch, I.; Elia, G.; Dawson, K. The Evolution of the Protein Corona around Nanoparticles: A Test Study. *ACS Nano* **2011**, *5*, 7503–7509.
66. Casals, E.; Pfaller, T.; Duschl, A.; Oostingh, G. J.; Puntes, V. Time Evolution of the Nanoparticle Protein Corona. *ACS Nano* **2010**, *4*, 3623–3632.
67. Doty, R. C.; Tshikhudo, T. R.; Brust, M.; Fernig, D. G. Extremely Stable Water-Soluble Ag Nanoparticles. *Chem. Mater.* **2005**, *17*, 4630–4635.
68. Spector, T. Refinement of the Coomassie Blue Method of Protein Quantitation: A Simple and Linear Spectrophotometric Assay for ≤0.5 to 50 Mg of Protein. *Anal. Biochem.* **1978**, *86*, 142–146.
69. Read, S. M.; Northcote, D. H. Minimization of Variation in the Response to Different Proteins of the Coomassie Blue G Dye-Binding Assay for Protein. *Anal. Biochem.* **1981**, *116*, 53–64.
70. Mosmann, T. Rapid Colorimetric Assay for Cellular Growth and Survival: Application to Proliferation and Cytotoxicity Assays. *J. Immunol. Methods* **1983**, *65*, 55–63.
71. Ralph, P.; Moore, M. A.; Nilsson, K. Lysozyme Synthesis by Established Human and Murine Histiocytic Lymphoma Cell Lines. *J. Exp. Med.* **1976**, *143*, 1528–1533.
72. Zhang, D.; Neumann, O.; Wang, H.; Yuwono, V. M.; Barhoumi, A.; Perham, M.; Hartgerink, J. D.; Wittung-Stafshede, P.; Halas, N. J. Gold Nanoparticles Can Induce the Formation of Protein-Based Aggregates at Physiological pH. *Nano Lett.* **2009**, *9*, 666–671.